UNSATCHEM: Unsaturated Water and Solute Transport Model with Equilibrium and Kinetic Chemistry

D. L. Suarez* and J. Šimůnek

ABSTRACT

Numerous models have been developed for predicting major ion chemistry in the soil zone and in recharge to groundwater. Soils that contain $CaCO_3$ are prevalent in arid and semiarid regions, as well as in humid and temperate regions that have been glaciated or contain carbonate bedrock. Under these conditions, carbonate–solution reactions and ion exchange are the dominant chemical processes. In this model we couple one-dimensional unsaturated water and solute transport with a major ion chemistry routine and plant water uptake. The model has several unique features, including expressions relating reductions in hydraulic conductivity to chemical factors, prediction of CO_2 partial pressure in the root zone based on a CO_2 production–multiphase transport submodel, kinetic expressions for silicate weathering, calcite precipitation–dissolution, and dolomite dissolution, representation of B adsorption using the constant capacitance model, a new method for predicting cation-exchange selectivity, the option to use Pitzer ion interaction expressions for high ionic strength, and a plant growth submodel that includes water, salinity, and O_2 stress. The chemical submodel considers equilibrium ion exchange, as well as various equilibrium and kinetic expressions for precipitation and dissolution of soil minerals, including gypsum, Mg carbonates, and sepiolite. The use of a predictive submodel for CO_2 production and transport allows for the calculation of CO_2 concentrations with depth and time. This enables us to avoid the assumption of constant CO_2 distribution or constant pH required by previous models. Use of kinetic expressions for carbonate chemistry allows a more realistic simulation of soil and groundwater solution composition as well as simulations of carbonate redistribution and climatic change with time.

MODELING THE TRANSPORT and concentration of major soluble ions in and below the root zone is a requisite for predicting groundwater quality as well as for managing irrigation and fertilization practices. Many models have been developed in the past 20 yr to quantify the physical and chemical processes that affect the transport of major ions. The hydrological models, solute transport models, and aqueous chemical equilibrium models were developed independently and only later were these three kinds of models coupled. Among these, Jury et al. (1978) developed a model for steady-state water flow in the unsaturated zone that considered ion exchange and calcite equilibrium. Schulz and Reardon (1983) presented a mixing cell analytical model for groundwater transport that considered steady-state water flow, and a simplified chemical model (no ion pairing or complexation) with ion exchange and calcite equilibria. Förster and Gerke (1988) proposed a multicomponent transport model based on steady-state water flux that considered a mobile–immobile water concept and carbonate equilibrium. Numerous other models have been developed for steady-state groundwater flow coupled with chemical equilibrium (Jennings et al., 1982; Walsh et al., 1984; Miller and Benson, 1983; Narasimhan et al., 1986; among others).

Simulation of soil water flow and soil chemical processes requires consideration of water and solute transport under variable water content conditions. Modeling of unsaturated water flow coupled to equilibrium chemistry has been undertaken by only a few researchers. Robbins et al. (1980a,b) combined an unsaturated water flow model with an ion exchange and carbonate chemistry and gypsum submodel that assumed fixed soil pH. Subsequently, Wagenet and Hudson (1987) developed a similar model that input fixed CO_2 at various depths instead of assuming fixed pH. Russo (1986) combined the solution chemistry of the Robbins et al. (1980a) model with the Bresler (1973) transport model. Yeh and Tripathi (1989, 1991) coupled a generalized chemical equilibrium model with unsaturated water flow. Application of the Yeh and Tripathi model to soil environments requires specification of total inorganic C and fixed pH. The model does not contain any provisions for plant water extraction. Šimůnek and Suarez (1994) developed a two-dimensional model with unsaturated water flow and major ion chemistry.

Evaluation of these models under field conditions is very limited. Only Robbins et al. (1980b) tested their model by comparing its results with experimental data obtained from a lysimeter study. However, in a field study, Dudley et al. (1981) indicated that the Robbins et al. (1980b) model could predict salinity, but not specific ion concentrations. These difficulties may be related to heterogeneous water flow, as mentioned by the researchers, but may also result from the assumptions of chemical equilibrium and fixed pH and the manner in which the calcite equilibrium is solved.

Most previous models assume chemical equilibrium

USDA-ARS, U.S. Salinity Lab., 450 W. Big Springs Rd., Riverside, CA 92507-4617. Received 2 Aug. 1996. *Corresponding author (dsuarez@ussl.ars.usda.gov)

Published in Soil Sci. Soc. Am. J. 61:1633–1646 (1997).

between the solution and the solid phases and require input of either CO_2 or pH with depth, without provision for time dependence or interaction with soil processes. The requirement that CO_2 be input leads to serious limitations to the utility of the models, especially in near-surface environments where climatic factors such as rainfall and temperature have an important influence on soil CO_2 concentrations. Several regression relations have been developed to predict average CO_2 from temperature, rainfall, or evapotranspiration. In addition to these factors, there are other factors that affect soil CO_2 concentrations, such as soil hydraulic properties and porosity (Suarez and Šimůnek, 1993). Also, average values do not consider the important effect of seasonal and short-term cycles at each site. Buyanovsky and Wagner (1983) measured seasonal changes in soil CO_2 concentration of 0.3 to 8% for cropped fields in Missouri. The CO_2 model developed by Šimůnek and Suarez (1993) was able to predict CO_2 production, transport, and distribution in the soil based on water inputs, soil hydraulic properties, potential evapotranspiration, and a production submodel.

The generally utilized assumption of mineral equilibrium is also only a rough approximation for soil and shallow groundwater environments. Suarez (1977a) measured calcite supersaturation of groundwaters beneath two irrigated regions. In both regions, waters were on average threefold supersaturated. Suarez et al. (1992) also determined calcite supersaturation in soil water sampled from the (water) unsaturated zone. The utility of a kinetic approach to improve prediction of major ion chemistry was shown by Suarez (1985), who presented results of simulations using steady-state unsaturated water flow combined with calcite precipitation kinetics using the Plummer et al. (1978) rate equations.

Existing models do not consider the effects of chemical properties on hydraulic conductivity. It is well documented, however, that low electrolyte concentration, high sodicity (McNeal, 1968; Frenkel et al., 1978), and elevated pH (Suarez et al., 1984) all adversely affect hydraulic conductivity. Consideration of these factors is essential to predicting water and solute movement in sodic soils.

Our objective was to develop a one-dimensional unsaturated water flow and solute transport model for predicting major ion and B chemistry in field environments, with emphasis on arid-zone chemistry, including the processes of plant water uptake, root and plant growth, and without the need for specifying the CO_2 or pH.

MODEL DEVELOPMENT

Water Flow

The Richards equation is used to describe one-dimensional water movement in partially saturated incompressible porous media:

$$\frac{\partial \theta}{\partial t} = \frac{\partial}{\partial z}\left[K\left(\frac{\partial h}{\partial z} + 1\right)\right] - Q \qquad [1]$$

where h is the water pressure head [L], θ is the water content [$L^3\ L^{-3}$], K is the hydraulic conductivity [$L\ T^{-1}$], t is time [T], z is the spatial coordinate [L] (vertically upward), and Q is the sink–source term [T^{-1}], which represents the water uptake rate by plant roots.

The unsaturated soil hydraulic properties are based on a set of closed-form equations (van Genuchten, 1980), using the capillary model of Mualem (1976) and modified here to account for the effects of chemistry on these properties. The soil water retention and hydraulic conductivity functions are given by

$$\theta(h) = \theta_r + \frac{\theta_s - \theta_r}{(1 + |\alpha h|^n)^m} \qquad [2]$$

and

$$K(h) = rK_sK_r = rK_sS_e^{1/2}[1 - (1 - S_e^{1/m})^m]^2 \qquad [3]$$

respectively, where

$$m = 1 - 1/n \qquad n > 1 \qquad [4]$$

$$S_e = \frac{\theta - \theta_r}{\theta_s - \theta_r} \qquad [5]$$

and where θ_r and θ_s denote residual and saturated water content [$L^3\ L^{-3}$], respectively, K_s is the saturated conductivity [$L\ T^{-1}$], K_r is the relative hydraulic conductivity, r is the chemical reduction function, S_e is relative saturation, and m, n, and α [L^{-1}] are the empirical parameters of the hydraulic characteristics. Hydraulic characteristics are determined by a set of six parameters: θ_r, θ_s, α, n, r, and K_s.

The chemical composition of the soil water and the exchangeable Na percentage have a dramatic effect on the soil hydraulic properties, as mentioned above. The hydraulic properties described by K_s and K_r are optimal values, inasmuch as the measurements are made under favorable chemical conditions. Numerous studies have documented that elevated levels of exchangeable Na, especially in combination with low electrolyte concentrations, will cause clay dispersion and/or swelling and subsequent reduction in soil hydraulic conductivity. In addition, Suarez et al. (1984) determined that elevated levels of pH have a very adverse effect on saturated hydraulic conductivity. The pH effects were determined from experiments in which the pH was varied at numerous fixed exchangeable Na and salinity levels. This allows separation of the pH effects from the salinity and Na effects. The overall chemical hydraulic reduction function, r, is given by

$$r = r_1r_2 \qquad [6]$$

where r_1 is the reduction due to salinity–sodicity interactions, and r_2 is the reduction due to adverse pH. The r_1 values are calculated for soils of California based on the experimental work of McNeal (1968), where

$$r_1 = 1 - \frac{v\epsilon^w}{1 + v\epsilon^w} \qquad [7]$$

where v and w are empirical factors, and ϵ is defined by

$$\epsilon = f_{\text{smectite}}\ 3.6 \times 10^{-2}\ \bar{x}_{Na}d^* \qquad [8]$$

where f_{smectite} is the weight fraction of smectite in the soil, d^* is an adjusted interlayer spacing, and $\bar{x}_{Na}$ is the Na charge fraction of the cation exchange. The reduction factor r_2, representing the effect of pH on hydraulic conductivity, is calculated from the experimental data of Suarez et al. (1984):

$$\begin{aligned} r_2 &= 1 && \text{for pH} < 6.83 \\ r_2 &= 3.46 - 0.36\text{pH} && \text{for pH} = 6.83 \text{ to } 9.3 \\ r_2 &= 0.1 && \text{for pH} > 9.3 \end{aligned} \qquad [9]$$

In view of the differences among soils, these specific values may not be generalized predictors of soil hydraulic conductivity but they do serve to illustrate the changes that occur in infiltration and solute movement under various chemical conditions. At the present time we assume that the hydraulic changes are reversible and that the water retention function is not affected by the solution composition. Information on these effects is not available at present.

Solute Transport Equation for Unsaturated Porous Media

The partial differential equation governing one-dimensional advective–dispersive chemical transport under transient flow in partially saturated porous media is taken as

$$\frac{\partial \theta c_{Ti}}{\partial t} + \rho \frac{\partial \bar{c}_{Ti}}{\partial t} + \rho \frac{\partial \check{c}_{Ti}}{\partial t} = \frac{\partial}{\partial z}\left[\theta D \frac{\partial c_{Ti}}{\partial z} - q c_{Ti}\right] \qquad i = 1, n_s \qquad [10]$$

where c_{Ti} is the total dissolved concentration of the aqueous component i [M L^{-3}], $\bar{c}_{Ti}$ is the total sorbed concentration of the aqueous component i [M M^{-1}], $\check{c}_{Ti}$ is the nonadsorbed solid-phase concentration of aqueous component i [M M^{-1}], ρ is the bulk density of the soil [M L^{-3}], D is the dispersion coefficient [L^2 T^{-1}], q is the volumetric flux [L T^{-1}], and n_s is the number of aqueous components. The coefficient D is the sum of the diffusion and dispersion components

$$D = \tau D_m + \lambda \frac{|q|}{\theta} \qquad [11]$$

where τ is the tortuosity factor, D_m is the coefficient of molecular diffusion [L^2 T^{-1}], and λ is the dispersivity [L]. The water flow, solute and CO_2 transport equations are solved using the Galerkin finite element method, as described in Šimůnek and Suarez (1993).

Equilibrium Chemistry

Each of the nine major aqueous components (Ca, Mg, Na, K, alkalinity, SO_4, Cl, B, and Si) is defined by summation of the individual species containing that component. For example Ca and B are defined by

$$Ca_T = [Ca^{2+}] + [CaSO_4^0] + [CaCO_3^0] + [CaHCO_3^+]$$
$$B_T = [B(OH)_3] + [B(OH)_4^-] \qquad [12]$$

where brackets represent concentrations. Alkalinity is defined by

$$\text{Alkalinity} = [HCO_3^-] + 2[CO_3^{2-}] + 2[CaCO_3^0] + [CaHCO_3^+] + 2[MgCO_3^0] + [MgHCO_3^+] + 2[NaCO_3^-] + [NaHCO_3^0] + [B(OH)_4^-] - [H^+] + [OH^-] \qquad [13]$$

The reactions in the CO_2–H_2O system and complexation reactions for major ions have been described in numerous publications, thus further discussion is not needed. A list of the variables and solids considered are given in Appendix A. The CO_2 partial pressure (pCO_2) is input to the chemical routine after calculation by the CO_2 production transport submodel. This subroutine is taken from the CO_2 model described in Šimůnek and Suarez (1993) and uses the parameters developed in Suarez and Šimůnek (1993).

The model considers both gas and aqueous-phase CO_2 transport and air–soil gas exchange and separate production–response functions for root respiration and microbial activity. These response functions consider temperature, water, and O_2 stress as well as plant growth. Heat transport and soil temperature are calculated as described in Šimůnek and Suarez (1993) using air temperature as an input. The model can be used for near-neutral to high pH environments as well as for representation of the addition of acid to calcareous soils (alkalinity can be negative, where the acid will dissolve calcite and pH increases quickly back to values where Al is not important). The model presently does not consider Al chemistry, thus is not suitable for simulations in which these reactions are important.

Precipitation of Calcite

The precipitation or dissolution of calcite in the presence of CO_2 can be described by the reaction

$$CaCO_3 + CO_2(g) + H_2O \rightleftharpoons Ca^{2+} + 2HCO_3^- \qquad [14]$$

where the solubility product K_{SP}^C is given by

$$K_{SP}^C = (Ca^{2+})(CO_3^{2-}) \qquad [15]$$

where parentheses denote activities. Substituting the equation for the dissociation of water, Henry's law equation for solubility of CO_2 in water, and the equations for the dissociation of H_2CO_3 in water (Eq. [A2], [A3], and [A4] in the appendix) we obtain:

$$(Ca^{2+})(HCO_3^-)^2 = \frac{K_{SP}^C K_{CO_2} K_{a1}}{K_{a2}} p_{CO_2} (H_2O) = K_{SP}^C K_T \qquad [16]$$

Rearranging and expressing in concentration yields the third-order equation

$$[Ca^{2+} + x][HCO_3^- + 2x]^2 = \frac{K_{SP}^C K_T}{\gamma_{Ca^{2+}} \gamma_{HCO_3^-}^2} \qquad [17]$$

where x is the quantity of calcite that must be dissolved or added to the solution in order to attain equilibrium. Solution of a second-order equation based on Eq. [15] will not converge properly, requiring up to 1000 iterations, as CO_3^{2-} is almost always a very minor species in solution. This problem is present in several currently utilized models.

Precipitation of Gypsum

The gypsum saturation status of a solution can be evaluated by comparing the ion activity product, IAP, to the K_{SP} where the IAP is defined by

$$[Ca^{2+}][SO_4^{2-}] = \frac{IAP}{\gamma_{Ca^{2+}} \gamma_{SO_4^{2-}} (H_2O)^2} \qquad [18]$$

To obtain equilibrium, i.e., when the IAP is equal to the solubility product K_{SP}^G, a quantity of gypsum must be added or removed from the solution. This quantity is obtained by solving the quadratic equation.

Magnesium Precipitation

We consider that Mg precipitation can occur as a carbonate (either nesquehonite or hydromagnesite) or as a silicate (sepiolite). Although there is still controversy as to which of the Mg carbonate phases is thermodynamically most stable, this is not of concern in this evaluation. Since we are developing a predictive model, we consider only phases that either precipi-

tate under earth surface conditions or occur frequently and are reactive under these conditions. Magnesite can thus be neglected, as it apparently does not form under earth surface temperatures, is relatively rare, and its dissolution rate is exceedingly small. Similarly, we do not consider precipitation of dolomite, as true dolomite appears to very rarely form in soil environments. Also, if dolomite is present in the soil, we do not assume that the soil solution will reach equilibrium with that solid. The dissolution rate of dolomite is very slow (Busenberg and Plummer, 1982), thus we incorporate kinetic expressions for dissolution.

Removal of substantial amounts of Mg by calcite precipitation (high Mg calcite) is possible at high Mg/Ca ratios but is not presently considered, as the precipitation kinetics, mineral stability, dependence of Mg substitution as a function of precipitation rate, and biological activity (which controls the Mg substitution) are unknown. If nesquehonite or hydromagnesite saturation is reached, the model will precipitate the predicted Mg carbonate. The Mg carbonate precipitated, combined with calcite precipitation, will probably represent the mixed Ca–Mg precipitate called *poorly ordered dolomite* or *protodolomite*. However, the resulting solution composition is much different than that produced by simply forcing equilibrium with respect to dolomite, as the model forms this mixed precipitate (calcite + Mg carbonate) under conditions of approximately three orders of magnitude supersaturation with respect to dolomite. This result is consistent with the high levels of dolomite supersaturation maintained in high Mg waters (Suarez, 1977, unpublished data). Precipitation (or dissolution, if present in the soil) of sepiolite is also considered by the model. Sepiolite will readily precipitate into a solid with a K_{SP} greater than that of well-crystallized sepiolite. Formation of this mineral requires high pH, high Mg concentrations, and low CO_2 partial pressure.

At 25°C and at CO_2 partial pressures above $10^{-3.27}$ kPa, nesquehonite is stable relative to hydromagnesite. The precipitation or dissolution of nesquehonite ($MgCO_3 \cdot 3H_2O$) in the presence of CO_2 is described by an equation similar to Eq. [14] with the solubility product K^N_{SP} defined by

$$K^N_{SP} = (Mg^{2+})(CO_3^{2-})(H_2O)^3 \quad [19]$$

Substituting Eq. [A2], [A3], and [A4] from the appendix, we obtain

$$(Mg^{2+})(HCO_3^-)^2 = \frac{K^N_{SP}K_{CO_2}K_{a1}}{K_{a2}}\frac{p_{CO_2}}{(H_2O)^2} = \frac{K^N_{SP}K_T}{(H_2O)^3} \quad [20]$$

We solve for equilibrium in a manner similar to that used for calcite, with a third-order equation. The precipitation or dissolution of hydromagnesite in the presence of CO_2 is described by

$$Mg_5(CO_3)_4(OH)_2 \cdot 4H_2O + 6CO_2(g) \rightleftharpoons 5Mg^{2+} + 10HCO_3^- \quad [21]$$

with the solubility product K^H_{SP} defined by

$$K^H_{SP} = (Mg^{2+})^5(CO_3^{2-})^4(OH^-)^2(H_2O)^4 \quad [22]$$

Substituting Eq. [A1], [A2], [A3], and [A4] from the appendix, we obtain

$$(Mg^{2+})^5(HCO_3^-)^{10} = \frac{K^H_{SP}K^6_{CO_2}K^6_{a1}p^6_{CO_2}}{K^4_{a2}K^2_w} = K^H_{SP}K_T \quad [23]$$

Again we solve for the amount to be precipitated or dissolved in the manner described for calcite and nesquehonite.

The precipitation or dissolution of sepiolite in the presence of CO_2 is described by

$$Mg_2Si_3O_{7.5}(OH) \cdot 3H_2O + 4.5H_2O + 4CO_2(g) \rightleftharpoons 2Mg^{2+} + 3H_4SiO_4^0 + 4HCO_3^- \quad [24]$$

with the solubility product K^S_{SP} defined by

$$K^S_{SP} = \frac{(Mg^{2+})^2(H_4SiO_4^0)^3(OH^-)^4}{(H_2O)^{4.5}} \quad [25]$$

Substituting Eq. [A1], [A2], and [A3] from the appendix, we obtain

$$(Mg^{2+})^2(HCO_3^-)^4 = \frac{K^S_{SP}K^4_{CO_2}K^4_{a1}p^4_{CO_2}(H_2O)^{4.5}}{K^4_w(H_4SiO_4^0)^3} = K^S_{SP}K_T \quad [26]$$

Relatively little information exists on the Si concentrations in soil waters, especially in arid zones. In soil systems, Si concentrations are controlled by dissolution (and possibly precipitation) of aluminosilicates and Si adsorption onto oxides and aluminosilicates. As a result of these reactions, Si concentrations in soil solution follow a U-shaped curve with pH. The data shown in Fig. 1 were obtained by reacting eight arid-zone soils from the western USA with deionized water at a soil/water ratio of 1:3 (by weight). For each soil, a series of samples were adjusted with either 0.1 *M* NaOH or 0.1 *M* HCl to achieve pH values in the range 7.5 to 11. Additional acid or base additions were made periodically to maintain pH. After 14 d, final pH values were measured and samples were filtered through 0.1-μm filters and Si analysis performed using the heteropoly blue method (Clesceri et al., 1989). The second-order regression equation

$$\Sigma SiO_2 = 0.001(6.34 - 1.43pH + 0.0819pH^2) \quad [27]$$

where SiO_2 is the sum of all silica species expressed in moles per liter, had an r value of 0.84 (Suarez, 1977b). This relationship probably provides only a rough estimate of Si concentrations, but we consider it acceptable because it is used only to restrain Mg concentrations at high levels of evapotranspiration, when Mg concentrations become very high at low CO_2 and high pH.

In this model, we utilize Eq. [27] to predict the Si concentrations in solution for arid-land soils when we utilize the sepiolite precipitation option. Freshly precipitated sepiolite has been prepared in the laboratory at IAP values of 10^{-35} comparable to the K_{SP} listed by Truesdell and Jones (1974), thus a kinetic expression for precipitation is not required.

An additional option (for nonalkaline soils) is to consider the Si concentration to be controlled by inputs from mineral weathering and concentrated only by processes of evapotranspiration. In this case we utilize kinetic expressions for the weathering of selected silicate minerals as discussed below.

Cation Exchange

Cation exchange between the solid phase and the solution can be described by the Gapon equation (White and Zelazny, 1986):

$$K_{ij} = \frac{\bar{c}_i^{z_i^+}}{\bar{c}_j^{z_j^+}}\frac{(\bar{c}_j^{z_j^+})^{1/z_j}}{(\bar{c}_i^{z_i^+})^{1/z_i}} \quad [28]$$

where z_i and z_j are the respective valences of species i and j and the overscored concentrations are those of the exchanger phase (in mol$_c$ kg^{-1} soil). We apply this equation for $\overline{Ca}$, $\overline{Mg}$, $\overline{Na}$, and $\overline{K}$ exchange, and a summation equation for the exchangeable ions:

$$\bar{c}_T = \overline{Ca}^{2+} + \overline{Mg}^{2+} + \overline{Na}^{+} + \overline{K}^{+} \quad [29]$$

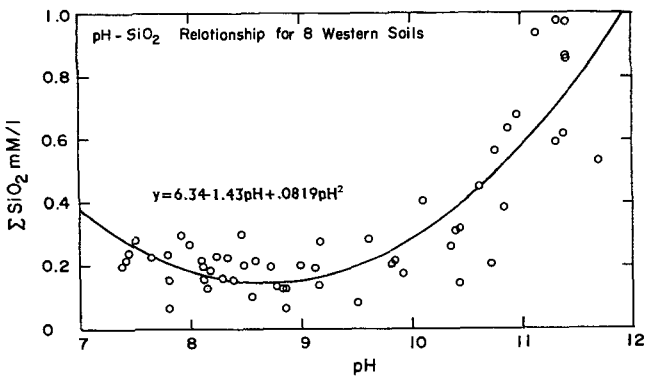

Fig. 1. Dissolved Si concentration as a function of pH for eight western U.S. arid-zone soils. Soils were reacted at 1:3 soil/water ratios for 14 d.

as done previously in Robbins et al. (1980b). It is assumed that the cation-exchange capacity $\bar{c}_T$ is constant.

Existing models either require input of a set of soil-specific selectivity values or use a generalized value. We observe that the experimentally determined selectivity values are not constant across the range of exchanger composition for any given soil and, further, that the variation from one soil to another can be large.

Recently, Suarez and Wood (1993) and Suarez et al. (1994) developed predictive models for Ca–Mg and Ca–Na exchange, respectively, that adequately predicted the ion selectivity for a range of smetitic soils. In their model, the selectivity value is calculated from knowledge of the cation-exchange capacity (CEC) and organic matter content, and using the known mineral and organic matter selectivities, constructing a mixing model for the overall selectivity. Initially the measured CEC is partitioned into organic and inorganic components. If the organic matter content is known, it is assumed that the CEC of the organic matter ($mol_c\ kg^{-1}$) is equal to its content in the soil ($kg\ kg^{-1}$) multiplied by its CEC. The calculations use a value of 4.9 $mol_c\ kg^{-1}$, the assumed CEC of pure organic matter (Pratt, 1957). The clay CEC is obtained by subtracting the organic matter CEC from the total. The resulting binary selectivity values are represented by expressions such as

$$K = \frac{[\bar{x}_{Ca_{clay}} + \bar{x}_{Ca_{om}}]}{[\bar{x}_{Mg_{clay}} + \bar{x}_{Mg_{om}}]} \frac{(Mg^{2+})}{(Ca^{2+})} \quad [30]$$

The system is defined by the following set of equations:

$$\bar{x}_{Ca_{om}} = \frac{CEC_{om} - \bar{x}_{Na_{om}} - \bar{x}_{K_{om}}}{\left[1 + \frac{1}{4.65(Ca^{2+})/(Mg^{2+})}\right]} \quad [31]$$

$$\bar{x}_{Ca_{om}} = \frac{CEC_{om} - \bar{x}_{Mg_{om}} - \bar{x}_{K_{om}}}{\left[1 + 10.0\frac{1}{(Ca^{2+})^{0.5}/(Na^{+})}\right]} \quad [32]$$

$$CEC_{om} = \bar{x}_{Ca_{om}} + \bar{x}_{Na_{om}} + \bar{x}_{Mg_{om}} + \bar{x}_{K_{om}} \quad [33]$$

$$\bar{x}_{Ca_{clay}} = \frac{CEC_{clay} - \bar{x}_{Na_{clay}} - \bar{x}_{K_{clay}}}{\left[1 + \frac{1}{1.10(Ca^{2+})/(Mg^{2+})}\right]} \quad [34]$$

$$\bar{x}_{Ca_{clay}} = \frac{CEC_{clay} - \bar{x}_{Mg_{clay}} - \bar{x}_{K_{clay}}}{\left[1 + \frac{1}{1.96(Ca^{2+})^{0.5}/(Na^{+})}\right]} \quad [35]$$

$$CEC_{clay} = \bar{x}_{Ca_{clay}} + \bar{x}_{Na_{clay}} + \bar{x}_{Mg_{clay}} + \bar{x}_{K_{clay}} \quad [36]$$

Table 1. Adjustable parameters for calculation of activity coefficients.

Species	a†	b†	a'
Ca^{2+}	5.0	0.165	
Mg^{2+}	5.5	0.20	
Na^{+}	4.0	0.075	
K^{+}	3.5	0.015	
SO_4^{2-}	5.0	−0.04	
CO_3^{2-}	5.4	0	
HCO_3^{-}	5.4	0	
$CaHCO_3^{+}$	6.0	0	
$MgHCO_3^{+}$	4.0	0	
H^{+}	9.0	0	
OH^{-}	3.5	0	
$H_3SiO_4^{-}$	5.4	0	
$H_2SiO_4^{2-}$	4.0		
$B(OH)_4^{-}$	2.5		
$CaCO_3^0$			−0.5
$CaSO_4^0$			−0.45‡
$MgCO_3^0$			−0.63‡
$MgSO_4^0$			−0.5
$H_4SiO_4^0$			−0.5

† Truesdell and Jones, 1974.
‡ Reardon and Langmuir, 1976.

The constants 4.65 and 1.10 represent the respective Ca–Mg selectivity constants for organic matter (Baes and Bloom, 1988) and smectite (Suarez and Zahow, 1989), while the constants 10.0 and 1.96 represent the respective Ca–Na selectivity constants for organic matter and smectite. In the absence of similar data on the Ca–K exchange selectivity, we utilize the exchange expression given above in Eq. [28] for both clay and organic matter. Use of these concepts results in a non-constant selectivity constant for the bulk soil, with decreased Ca selectivity with increasing exchangeable Ca values (at the low range of exchangeable Ca values, consistent with experimental data). We utilize this exchange model whenever the soil organic matter content is known.

Activity Coefficients

At low to moderate ionic strength, we calculate activity coefficients with an extended version of the Debye–Hückel equation (Truesdell and Jones, 1974)

$$\ln \gamma = -\frac{Az^2\sqrt{I}}{1 + B\sqrt{I}} + bI \quad [37]$$

where A and B are constants depending only on the dielectric constant, solution density, and temperature, z is the ionic charge, a and b are adjustable parameters fit to mean salt activity coefficients, and I is the ionic strength. The adjustable parameters a and b for individual species are listed in Table 1. The activities of neutral species are calculated as

$$\ln\gamma = a'I \quad [38]$$

where a' is an empirical parameter whose values are given in Table 1.

At high ionic strength ($I > 0.1\ m$) activity coefficients are not simply universal functions of ionic strength, but are dependent on specific ion interactions (Felmy and Weare, 1986). Activity coefficients are now expressed in a virial-type expansion of the form (Pitzer, 1979)

$$\ln\gamma_i = \ln\gamma_i^{DH} + \sum_j B_{ij}(I)m_j + \sum_j \sum_k C_{ijk}m_j m_k + \ldots \quad [39]$$

where m_i is the molality, γ_i^{DH} is a modified Debye–Hückel activity coefficient, which is a universal function of ionic strength, and B_{ij} and C_{ijk} are specific coefficients for each ion–ion interaction. The specific form of this equation for cations, anions, and neutral species is adopted from Felmy and Weare (1986).

Table 2. Temperature-dependent thermodynamic constants.

Constant	a_1	a_2	a_3	a_4	a_5	References
log K CO_2	108.3865	−6 919.53	0.01985076	−40.45154	669 395	Plummer and Busenberg (1982)
log K_{a_1} H_2CO_3	−356.3094	21 834.37	−0.06091964	126.8339	−1 684 915	Plummer and Busenberg (1982)
log K_{a_2} H_2CO_3	−107.8871	5 151.79	−0.03252849	38.92561	−563 713.9	Plummer and Busenberg (1982)
log K $CaCO_3^0$	1228.732	−35 512.75	0.299444	−485.818	0	Plummer and Busenberg (1982)
log K $CaSO_4^0$	−1.24	0	−0.0036	0	0	Bell and George (1953)
log K $CaHCO_3^+$	−1209.120	34 765.05	−0.31294	478.782	0	Plummer and Busenberg (1982)
log K $MgCO_3^0$	21.39	−3 265	−0.04467	0	0	Reardon and Langmuir (1974)
log K $MgSO_4^0$	0.95	0	−0.011	0	0	Jacobson (1973)
log K $MgHCO_3^+$	76.344	−11 132.0	−0.1338	0	0	Reardon (1974, p. 85)
log A	−1.15083	93.642	0.001830	0	0	Robinson and Stokes (1965)
log B	−0.76645	30.7702	0.0006058	0	0	Robinson and Stokes (1965)
log K_w	6.0875	4 470.99	0.01705	0	0	Stumm and Morgan (1981)
log K calcite	−171.9065	2 839.319	−0.077993	71.595	0	Plummer and Busenberg (1982)

Temperature Dependence

Most of the equilibrium constants used in this model have been determined as a function of temperature. Where available, the equilibrium constants are expressed as a power function of the absolute temperature:

$$\log K = a_1 + \frac{a_2}{T} + a_3 T + a_4 \log T + \frac{a_5}{T^2} \quad [40]$$

Table 2 lists the temperature-dependent thermodynamic constants used in the calculations.

The temperature dependence of the equilibrium values for which the constants of Eq. [40] do not exist are calculated from the enthalpy of reaction (Table 3).

Kinetic Model of Calcite Precipitation–Dissolution

Calcite precipitation–dissolution kinetic models are almost all based on the assumption that the reaction rate is dependent on the surface area of the calcite. The dissolution–precipitation model of Plummer et al. (1978) is the most comprehensive model for pure systems, based on dissolution studies across a wide range in pH (2–7.0) and CO_2 pressure (35 Pa–100 kPa). The calcite dissolution in the absence of dissolved organic carbon (DOC) is thus calculated with the rate equation of Plummer et al. (1978):

$$R^C = k_1 (H^+) + k_2 (H_2CO_3^*) + k_3 (H_2O) - k_4 \frac{K_{a2}}{K_{SP}^C} (Ca^{2+})(HCO_3^-) \quad [41]$$

$$k_4 = k_1' + \frac{1}{(H_S^+)}[k_2 (H_2CO_3^*) + k_3 (H_2O)] \quad [42]$$

where at 25°C, $k_1 = 0.051$, $k_2 = 3.45 \times 10^{-5}$, $k_3 = 1.18 \times 10^{-7}$, and $k_1' = 0.051$. The dissolution–precipitation rate R^C is expressed in millimoles of calcite per square centimeter of surface area per second. The term (H_S^+) is the H^+ activity at the calcite surface. It is assumed to be (H^+) at calcite saturation where pCO_2 at the surface equals pCO_2 in the bulk solution. The temperature dependence of the constants k_1, k_2, and k_3 is expressed as

$$\log k_i = a_1 + \frac{a_2}{T} \qquad i = 1, 2, 3 \quad [43]$$

where the constants are given in Table 4. For conditions where pH > 8 and pCO_2 < 1.01 kPa, the Plummer et al. (1978) equation underestimates the precipitation rate (Suarez, 1983; Inskeep and Bloom, 1985); thus the following expression is used (Inskeep and Bloom, 1985):

$$R^C = -11.82[(Ca^{2+})(CO_3^{2-}) - K_{SP}^C] \quad [44]$$

with an apparent Arrhenius activation energy of 48.1 kJ mol^{-1} for the rate constant.

The above relationships for calcite crystal growth are based on a clean calcite surface in the absence of "surface poisons". The inhibiting effects of DOC on calcite precipitation is well established and related to surface adsorption of DOC. Inskeep and Bloom (1986) reported data on the effect of water-soluble organic C on calcite crystal growth. From their data, we developed the following predictive relationship for reduction in calcite precipitation due to the presence of DOC:

$$r = \exp(-a_1 x - a_2 x^2 - a_3 x^{0.5}) \quad [45]$$

where r is the reduction constant, x is the DOC (μmol L^{-1}) and a_1, a_2, and a_3 are the nonlinear regression coefficients (0.005104, 0.000426, and 0.069111, respectively). This relation, as shown in Fig. 2, provided excellent prediction, with a correlation coefficient of 0.998. The reduction constant, r, is then multiplied by the R^C values calculated with either Eq. [41] or

Table 3. Temperature dependence of equilibrium constants (Truesdell and Jones, 1974).

Species	K	ΔH_r^0 (289.15°K)
		J mol^{-1}
Aqueous	K_a†	
$NaCO_3^-$	0.0540	−37 337
$NaSO_4^-$	0.1200	−4 693
$NaHCO_3^0$	0.562	–
KSO_4^-	0.1413	−9 428
$H_3SiO_4^-$	1.175×10^{-10}	37 437
$H_2SiO_4^{2-}$	2.404×10^{-22}	124 502
$B(OH)_4^-$	5.75×10^{-10}	−42 400
Solid	K_{sp}	
Gypsum	2.512×10^{-5}‡	1 131
Hydromagnesite	1.730×10^{-37}	−106 930
Nesquehonite	2.393×10^{-6}	−28 366
Sepiolite	3.138×10^{-38}	–

† K_a association.
‡ Ball et al., 1987.

Table 4. Temperature dependence of kinetic constants of calcite (Plummer et al., 1978) and dolomite (Busenberg and Plummer, 1982).

	a_1	a_2
	Calcite	
k_1	0.198	−444
k_2	2.84	−2177
k_3 (T < 298.15)	−5.86	−317
k_3 (T > 298.15)	−1.1	−1737
	Dolomite	
k_1	2.12	−1880
k_2	−0.07	−1800
k_3	0.53	−2700
k_4†	3.16	−2300
k_4	7.34	−3700

† For $FeCO_3$ < 0.007.

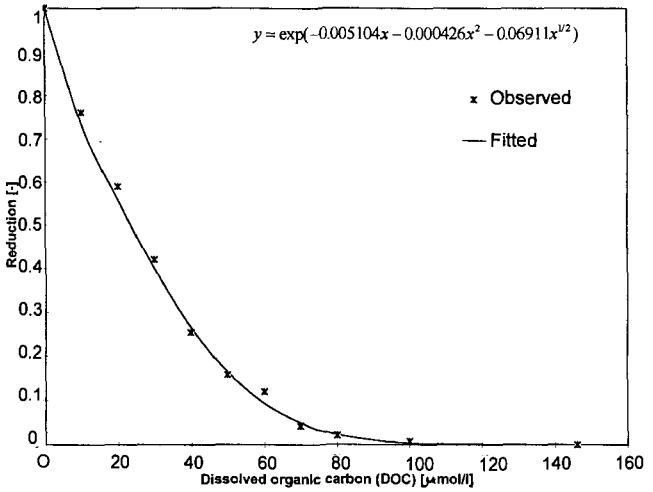

Fig. 2. Relationship between reduction in calcite precipitation and dissolved organic carbon (DOC). Data are taken from Inskeep and Bloom (1986).

[44] to obtain the predicted rate constant in the presence of the specified DOC concentration.

These and other calcite rate models all consider reaction rates to be proportional to surface area. For simulation of calcite dissolution in natural systems, these models may be suitable, after adjustment for the poisoning of the surface, as discussed above. However, these rate models may not be suitable for predicting calcite precipitation rates, as the concentrations of DOC in natural environments are usually comparable to levels found by Inskeep and Bloom (1986) to completely inhibit calcite crystal growth.

Recently Lebron and Suarez (1996) developed a precipitation rate model that considers the effects of DOC on hetergeneous calcite nucleation. In the presence of clay, the rate R_T is equal to the sum of the crystal growth rate and heterogeneous nucleation rate, where

$$R_{CG} = k_{CG}S_c[(Ca^{2+})(CO_3^{2-}) - K_{SP}] \times [0.14 - 0.11 \log \text{DOC}] \quad [46]$$

and

$$R_{HN} = k_{HN}0.02S \log[\Omega - 2.5][3.37 \times 10^{-1.14}\text{DOC}] \quad [47]$$

where k_{CG} = 64.8 mmol s^{-1} m^{-2}, S_c is the calcite surface area (m^2 L^{-1}), k_{HN} = 7.82 × 10^{-4} s^{-1} m^{-2}, S is the total soil surface area (m^2 L^{-1}), DOC is expressed in mmol L^{-1}, Ω = IAP/K_{SP}, and R_{HN} is the precipitation rate (mmol L^{-1} s^{-1}). The value 0.02S represents the active sites related to the total surface area. This value is given for illite and may vary with mineralogy. This equation leads to calcite precipitation rates that are independent of the calcite surface area when DOC >0.05 mM, consistent with the experimental data of Lebron and Suarez (1996). This model considers heterogeneous calcite nucleation (on clay surfaces) with poisoning of the crystals upon formation. We consider Eq. [47] to be the most realistic for precipitation in root-zone environments while Eq. [44] and [45] are most suitable for dissolution. The use of the Plummer et al. (1978) equation is suitable only for very low DOC environments (<0.01 mM).

Kinetic Model of Dolomite Dissolution

The reaction rates of dolomite dissolution were calculated with the rate equation of Busenberg and Plummer (1982) for sedimentary dolomites:

$$R^D = k_1(H^+)^{0.5} + k_2(H_2CO_3^*)^{0.5} + k_3(H_2O)^{0.5} - k_4(HCO_3^-) \quad [48]$$

where the temperature dependence of the constants k_1, k_2, k_3, and k_4 is expressed by Eq. [43] (Table 4). The precipitation rate R^D is expressed in millimoles of dolomite per square centimeter of dolomite surface area per second. According to Busenberg and Plummer (1982), the reaction rate became so low above IAP values of 10^{-20} that the rate could not be measured within the time frame of their experiments. In the absence of data at low levels of undersaturation, we extrapolate their results to IAP = 10^{-19} and assume that the reaction rate is negligible above that value. As a result, dolomite equilibrium in the model is never achieved by dissolution, but equilibrium or supersaturated values can result from decreases in pCO_2 or by concentration of salts by evapotranspiration. In the absence of data specific to dolomite, we utilize the calcite reduction constants for the effect of organic matter on dissolution rates.

Kinetic Model of Silicate Mineral Dissolution

Although silicate mineral dissolution rates are orders of magnitude slower than calcite dissolution, they nonetheless are extremely important for predicting base cation concentrations in noncalcareous soils and for assessing sensitivity to soil acidification, either by natural processes or by acid rain. Several different rate expressions have been used for feldspar dissolution, the most successful of which are variations of the Furrer and Stumm (1986) model:

$$R_t = R_H + R_L$$
$$R_H = k_H(C_H^S)^n$$
$$R_L = k_L C_L^S \quad [49]$$

where R_H and R_L are the proton- and ligand-promoted rates, k_L and k_H are the rate constants, C_H^S and C_L^S are, respectively, the surface concentrations of protons and ligands, and n is the order of the reaction. This model, developed for oxides, is not able to simulate the silicate dissolution rates in the pH range 3 to 8 (Amrhein and Suarez, 1988). Amrhein and Suarez (1988) modified this equation by adding a rate term proportional to the uncharged surface silanol groups and substituting the term Γ, which represents the sum of the proton and hydroxyl sites, for the term C_H^S in Eq. [49]. Combining the surface proton and hydroxyl sites into one expression was justified by the essentially equal effects of the two surface groups on the dissolution rates of plagioclase feldspars. This has been determined experimentally in the work of Chou and Wollast (1985) for albite and Amrhein and Suarez (1988) for anorthite, representing the end members in the plagioclase feldspar series. However, other studies indicate that this equality cannot be generalized, thus we use the modified rate equation

$$R_t = a(\Gamma)^{4.0} + a'(\Gamma')^{4.0} + b_1(\text{SOH}) + b_2(\text{S-L}) \quad [50]$$

where a, a', b_1, and b_2 are the rate coefficients for the proton, hydroxyl, neutral, and surface-ligand sites and Γ, Γ', SOH, and S-L are the surface concentrations of proton, hydroxyl, neutral, and surface-ligand sites. Detailed rate data for use with Eq. [50] are not available for all silicates; however, in the pH range of 5 to 9, this equation can often be simplified to

$$R_t = b_1(\text{SOH}) + b_2(\text{S-L}) \quad [51]$$

where b_1 and b_2 are equal to 2.09 × 10^{-8} and 4.73 × 10^{-6} s^{-1}, respectively, for anorthite, and SOH, the total number of surface sites, is taken as 0.12 mmol m^{-2} (Amrhein and Suarez,

1988) when R_t is expressed in mmoles per square meter per second.

Using the rate model expressed in Eq. [51], and in that restricted pH range, we consider the following reactions for anorthite, labradorite, albite, K feldspar, biotite, and hornblende:

$$CaAl_2Si_2O_8 + H_2CO_3 + H_2O \rightarrow Ca^{2+} + 2HCO_3^- + \text{kaolinite} \quad [52]$$

$$4Ca_{0.5}Na_{0.5}Al_{1.5}Si_{2.5}O_8 + 6H_2CO_3 + 11H_2O \rightarrow 2Ca^{2+} + 2Na^+ + 6HCO_3^- + 3\text{kaolinite} + 4H_4SiO_4 \quad [53]$$

$$2NaAlSi_3O_8 + 2H_2CO_3 + 9H_2O \rightarrow 2Na^+ + 2HCO_3^- + \text{kaolinite} + 4H_4SiO_4 \quad [54]$$

$$2KAlSi_3O_8 + 2H_2CO_3 + 9H_2O \rightarrow 2K^+ + 2HCO_3^- + \text{kaolinite} + 4H_4SiO_4 \quad [55]$$

$$2KMg_3AlSi_3O_{10}(OH)_2 + 14H_2CO_3 + H_2O \rightarrow 2K^+ + 6Mg^{2+} + 14HCO_3^- + \text{kaolinite} + 4H_4SiO_4 \quad [56]$$

$$Ca_2Mg_4Al_2Si_7O_{22}(OH)_2 + 12H_2CO_3 + 5H_2O \rightarrow 2Ca^{2+} + 4\,Mg^{2+} + 12HCO_3^- + \text{kaolinite} + 5H_4SiO_4 \quad [57]$$

Values for these silicate minerals are taken from the studies of Swoboda-Colberg and Drever (1993) and Suarez and Wood (1996), based on long-term weathering studies in experiments that minimized the effects of grinding and pretreatment artifacts.

An alternative approach is the rate model of Sverdrup and Warfvinge (1988):

$$R = k_H + \frac{[H^+]^n}{[M]^x[Al^{3+}]^y} + \frac{kH_2O}{[Al^{3+}]^u} + k_{CO_2}\,p_{CO_2} + k_{org}[org]^{0.5} \quad [58]$$

where k is the reaction rate for the different processes, and n, x, y, u, and m are the reaction orders, all determined experimentally. We utilize the field values given by Sverdrup and Warfvinge (1988).

Adsorption

Transport of minor element anions such as B, As, and Se is often affected by adsorption processes. Various modeling approaches have been used in the past, ranging from retardation factors to the use of Langmuir isotherms. These models generally require the input of adsorption isotherm values specific to a given pH. In this model, we utilize the constant capacitance model, since it is able to represent the effect of pH on adsorption affinity, and our model has the capacity to predict soil solution pH. The model contains the following assumptions: adsorption is a ligand-exchange mechanism, all surface complexes are inner sphere, and no surface complexes are formed with other salts in solution. The relation between the surface charge and the surface potential is given by

$$\sigma = \frac{CSa}{F}\Psi \quad [59]$$

where C is the capacitance density (F m^{-2}), S is the specific surface area (m^2 g^{-1}), a is the suspension density (g L^{-1}), F is the Faraday constant (C mol$_c^{-1}$), Ψ is potential (V), and σ is expressed in mol$_c$ L^{-1}. The intrinsic conditional equilibrium constants corresponding to B adsorption are (Goldberg and Glaubig, 1985)

$$K_+ = \frac{[SOH_2^+]}{[SOH][H^+]}\exp[F\Psi/RT] \quad [60]$$

$$K_- = \frac{[SO^-][H^+]}{[SOH]}\exp[-F\Psi/RT] \quad [61]$$

$$K_B = \frac{[SH_2BO_3]}{[SOH][H_3BO_3]} \quad [62]$$

The mass balance equations for the surface functional groups and B are given by

$$[SOH]_T = [SOH] + [SOH_2^+] + [SO^-] + [SH_2BO_3] \quad [63]$$

$$B_T = H_3BO_3 + SH_2BO_3 \quad [64]$$

and the charge balance equation for the surface is defined by

$$\sigma = [SOH_2^+] - [SO^-] \quad [65]$$

In the absence of soil-specific data, we utilize the average soil constants of 9.3, −10.6, and 5.5 for the values of log K_+, log K_-, and log K_B, respectively (Goldberg, 1993). We utilize the value of 1.06 F m^{-2} for the capacitance (C). Using the data of Goldberg and Glaubig (1985), we developed the following expression relating the experimentally determined adsorption site density to S, the soil surface area:

$$[SOH]_T = 2.53 \times 10^{-7} + 4.61 \times 10^{-9}\,S \quad [66]$$

where S is expressed in square meters per gram and adsoption density is in moles per gram. As shown in Fig. 3, this expression provides a satisfactory prediction of B adsorption density as a function of total surface area. In contrast to direct determination of adsoprtion density, which requires time-consuming adsorption experiments, surface area can be determined relatively rapidly or estimated from mineralogy and clay content. The relation given by Eq. [66] had an r value of 0.96 (n = 14). By inputting a soil surface area and calculating suspension density a from water content and bulk density, the system is now defined by seven equations and seven unknowns.

The numerical solution of the chemical system is made using an iterative approach similiar to that utilized in WATEQ (Truesdell and Jones, 1974), except with the addition of solid- and sorbed-phase reactions. Initial calculation is made of ionic strength, temperature-dependent constants, and activity coefficients. Calculation is then made of pH from charge balance and partioning of alkalinity into HCO_3 and CO_3 by solving Eq. [A1] to [A4] and equilibrating the solution composition with the solid phases. The iteration criterion in this section is the second dissociation of H_2CO_3. After passing this criterion, the major ion concentrations are redistributed into the ion pairs and complexes. Each component is checked for mass balance (i.e., Eq. [12]). After iteration, the sorbed phases are now equilibrated with the solution, and mass and charge balance checked. The process is repeated until specified convergence is achieved (typically set at 0.1%). Overall convergence criteria include charge balance and change in ionic strength.

RESULTS AND DISCUSSION

Unique features of the model are demonstrated in the following simulations. In the first simulation, we

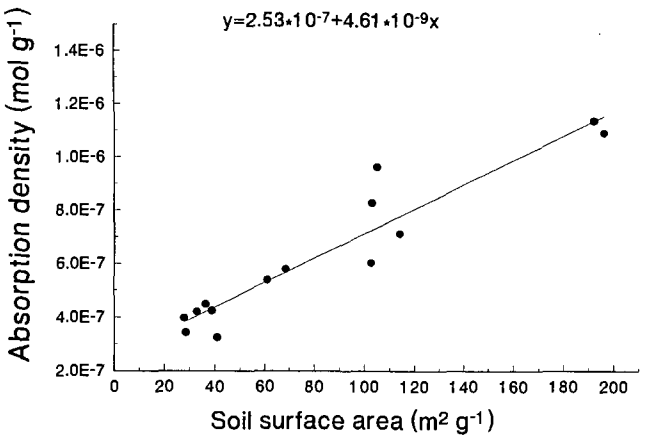

Fig. 3. Relationship between B absorption density and soil surface area for 14 western U.S. arid-zone soil samples. Data taken from Goldberg and Glaubig (1985).

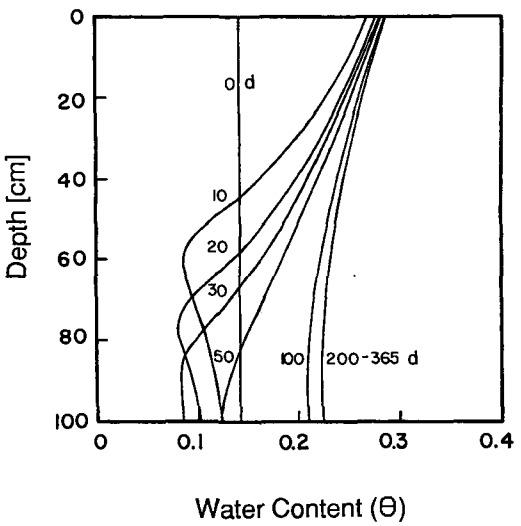

Fig. 4. Soil water content profiles with depth for 365-d simulation of irrigation and plant water uptake using Wellton Mohawk drainage water as the irrigation source.

examine differences in solution composition and location of precipitation when simulating calcite precipitation using a kinetic as compared with an equilibrium model. We specify irrigation with a Colorado River derived well water, which is already calcite supersaturated (drainage well no. 15 from the Wellton–Mohawk Irrigation District in Arizona, as analyzed by Suarez [1977a]). The soil CO_2 distribution is taken as atmospheric at the soil surface, increasing linearly to 2 kPa (2%) at the bottom of the root zone. In this example, the water uptake distribution by plants is also linearly scaled from the maximum at the soil surface to zero at the bottom of the soil root zone (100 cm). The initial volumetric water content is 0.143 $m^3\ m^{-3}$. We assume a constant irrigation of 1 cm d^{-1} and a plant water uptake of 0.9 cm d^{-1}. In this example, we neglect ion exchange in order to evaluate differences due to the kinetic and equilibrium assumptions. The unsaturated hydraulic conductivity–water content relationship was calculated using the equation of van Genuchten (1980) from the water content–pressure head data given in Hillel and van Bavel (1976).

Figure 4 shows that the water content in the soil increased with time and was close to steady state after 100 d. The decrease in water content with depth is due to plant root extraction of water. The Ca concentration profile using the equilibrium model, shown in Fig. 5a, increases steadily with time, reaching steady state after 100 d. After 100 d, the concentration ranges from 6 $mmol_c\ L^{-1}$ at the surface to 32 $mmol_c\ L^{-1}$ at the 60-cm depth. Using the kinetic model with an assumed calcite surface area of $1 \times 10^{-7}\ m^2\ m^{-3}$ of soil, Ca concentrations are almost doubled near the surface and similar to the equilibrium case at the bottom of the profile. The Ca values are roughly similar at the bottom of the soil profile because of gypsum precipitation at the lower depths, discussed below. The simulated output for the kinetic model is dependent on the surface area value

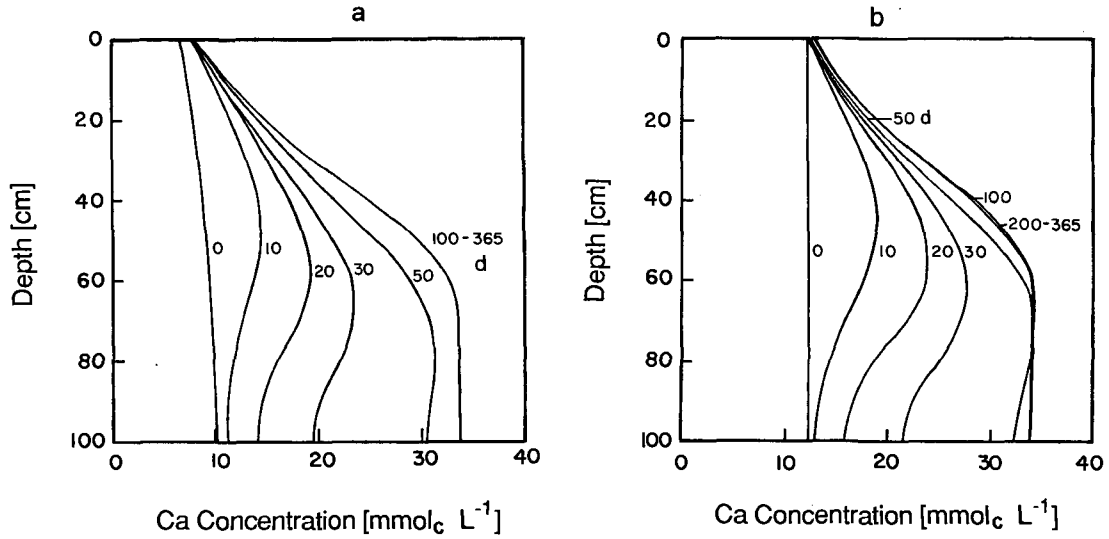

Fig. 5. Calcium concentration profiles with depth for 365-d simulation of irrigation and plant water uptake using Wellton Mohawk drainage water and (a) calcite equilibrium condition and (b) kinetic model with calcite surface area taken as $1 \times 10^{-7}\ m^2\ m^{-3}$ of soil.

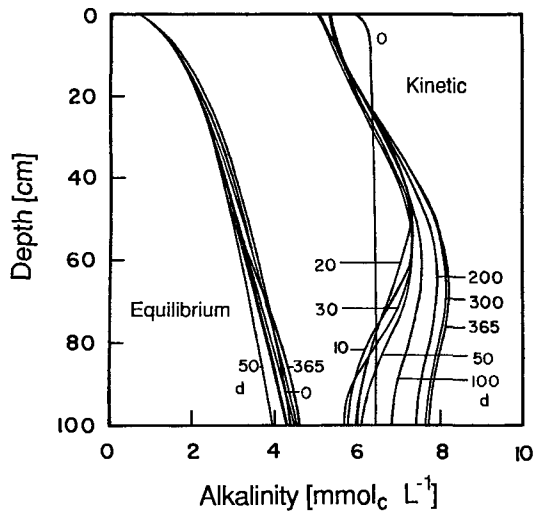

Fig. 6. Alkalinity concentration profiles with depth for 365-d simulation of irrigation and plant water uptake using Wellton Mohawk drainage water and calcite equilibrium condition compared with kinetic model with calcite surface area taken as 1×10^{-7} m^2 m^{-3} of soil.

and DOC content of the soil water. In this case, we did not include DOC.

The alkalinity values shown in Fig. 6 indicate large differences between the two simulations, with the kinetic model again predicting much larger concentrations, especially in the shallow depths but still twice as large at the bottom of the profile. These alkalinity differences are related to the calcite supersaturation throughout the soil profile, as shown in Fig. 7, which shows the pIAP values for calcite as a function of depth and time. The final steady-state pIAP values range around 7.0 in the near-surface environment to 8.1 at the 100-cm depth, similar to those reported by Suarez (1985). In contrast, the equilibrium model results in

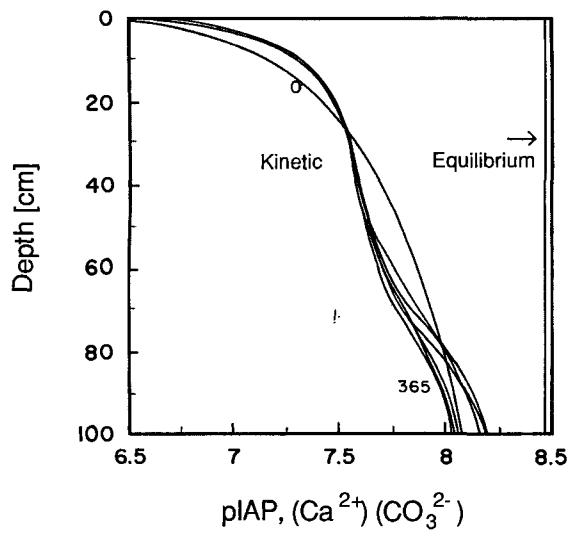

Fig. 7. Calcium carbonate pIAP (ion activity product) values with depth for 365-d simulation of irrigation and plant water uptake using Wellton Mohawk drainage water. Line at pIAP = 8.48 represents value for equilibrium condition and curved lines represent values obtained using the kinetic model with a calcite surface area of 1×10^{-7} m^2 m^{-3} of soil.

calcite equilibrium (pIAP = 8.47) at all times and locations in the profile.

Due to the initial equilibrium assumption, the kinetic simulation took longer to reach steady state, as evident by the pIAP–time relations in Fig. 7, as well as the comparison of alkalinity–time relations in Fig. 6. In addition to differences in solution composition, the models also give differences in the carbonate distribution with depth, as shown in Fig. 8a and 8b. The equilibrium model predicts a large quantity of calcite precipitation in the first depth followed by a very large quantity of calcite dissolution in the shallow depths, followed by slight precipitation at depth. This unrealistic result demonstrates the limitations of an equilibrium model for simulation of calcite precipitation. The result can be partially avoided by the equally unrealistic forcing of the input solution to calcite saturation before initiating the program. In contrast to the equilibrium model, the kinetic model simulates a condition of decreasing precipitation with depth. The predicted distribution depends on various factors including the calcite saturation status of the input water, amount of water applied, CO_2 distribution with depth, plant water uptake and distribution with depth, as well as potential gypsum precipitation, which in this case limits calcite precipitation at depth. Quantity and depth of calcite precipitation in soil profiles has been used in various simplified equilibrium models for reconstruction of paleoclimate as well as for pedogenesis. While simplified models may be needed for regional-scale climatic simulations, nonetheless, a detailed mechanistic model provides the opportunity to examine the sensitivity of the results to input assumptions. In addition this example illustrates the importance of kinetic factors on calcite distribution — equilibrium models will not yield realistic distributions.

Gypsum precipitation using the calcite kinetic model is simulated as occurring in the 60- to 100-cm zone, with a maximum at 67 cm. In contrast, with the equilibrium model, the location of gypsum accumulation is shifted downward, due to the smaller Ca and alkalinity concentrations for the equilibrium than for the kinetic model.

The second example considers both the interaction of transient water flow and water content, as well as the dynamic CO_2 submodel (Šimůnek and Suarez, 1993), with the equilibrium and kinetic carbonate subroutines. In these simulations we considered intermittent irrigation of 10 cm, every 10 d, of Colorado River water (where Ca = 2.63, Mg = 1.03, Na = 2.55, Cl = 1.94, alkalinity = 2.33, and SO_4 = 2.0 mmol$_c$ L^{-1}). Although the model can calculate CO_2 production as a function of environmental stress, for the purposes of comparing the different simulations we fixed the CO_2 production at 0.007 m^3 m^{-2}, which is a realistic field value (Suarez and Šimůnek, 1993). Other conditions are those given for the previous example.

After 100 d, a steady-state cycle was reached in that the water content and solution composition cycled between irrigations. Shown in Fig. 9 is the water content distribution with depth for a 10-d interval between irrigations after 300 d of simulation. After irrigation, the water content increases in the shallow soil zone with

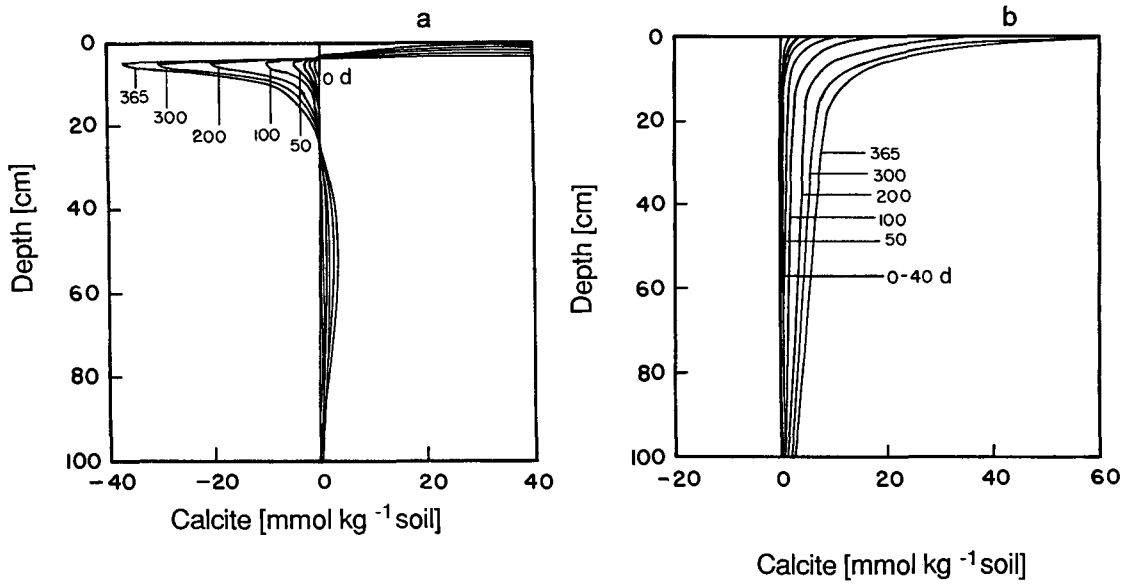

Fig. 8. Quantity of calcite precipitated (+) or dissolved (−) with depth for 365-d simulation of irrigation and plant water uptake using Wellton Mohawk drainage water and (a) calcite equilibrium condition and (b) kinetic model with calcite surface area taken as 1×10^{-7} m^2 m^{-3} of soil.

subsequent redistribution and water uptake by plants. Ten days after an irrigation, the water content is back to the initial conditions immediately before the next irrigation. Using the dynamic CO_2 production transport model, we simulate changing CO_2 concentrations with depth and time. As shown in Fig. 10, the CO_2 concentrations are greatest 2 d after an irrigation when the water content near the surface is still high. High water content resticts gas diffusion, and after sufficient time restricted diffusion results in elevated CO_2 concentrations. Upon drainage, the soil CO_2 distribution quickly reverts back to the pattern shown on Days 4 through 10, with increasing CO_2 concentration with depth to the bottom of the root zone. These dynamic distributions with space and time in turn produce effects on the soil solution composition.

The simulations in Fig. 11 show that the Ca concentration is relatively constant during the 10-d cycle using the equilibrium model at fixed CO_2. Increasing concentration with depth due to root water uptake is moderated by calcite precipitation. In contrast, the Ca concentrations changed with time by more than a factor of two in the upper portion of the profile when the kinetic model was utilized. The kinetic model also predicts higher concentrations throughout the profile. At shallow depths, this is due to both calcite supersaturation and fluctuations in CO_2; in the lower portions of the profile it is primarily due to calcite supersaturation during precipitation. The corresponding alkalinity concentrations for the same two simulations are shown in Fig. 12. Similar to the Ca profiles, the alkalinity concentrations and changes with time are greater using the kinetic model than the equilibrium model. The alkalinity concentrations with time in the equilibrium simulation

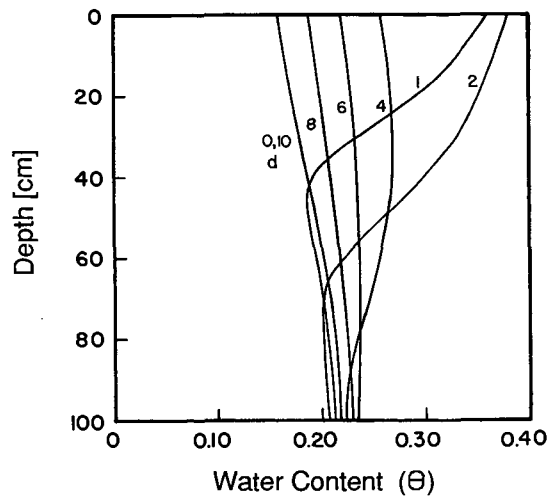

Fig. 9. Soil water content profiles with depth for a 10-d irrigation cycle after 1-yr simulation of irrigation and plant water uptake using Colorado River water.

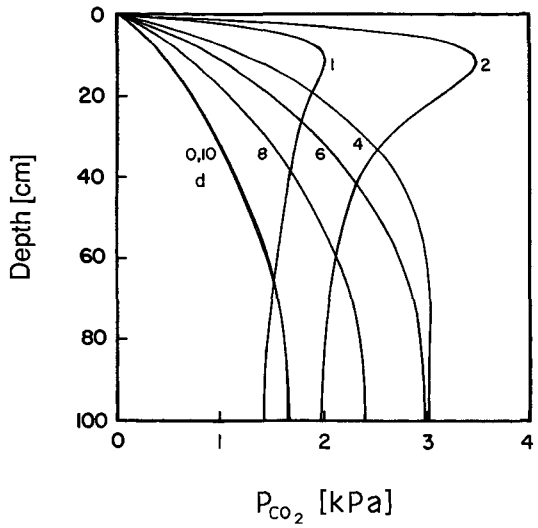

Fig. 10. Soil CO_2 partial pressure profiles with depth for a 10-d irrigation cycle after 1-yr simulation of irrigation and plant water uptake using Colorado River water. Simulation uses the CO_2 production–transport submodel.

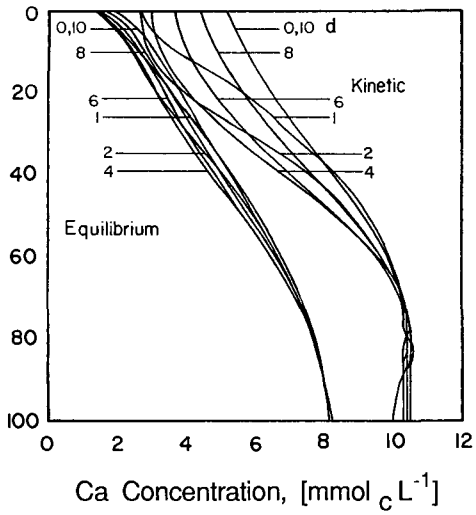

Fig. 11. Calcium concentration profiles with depth for a 10-d irrigation cycle after 1-yr simulation of irrigation and plant water uptake using Colorado River water (a) calcite equilibrium condition and (b) kinetic model coupled to CO_2 production–transport submodel.

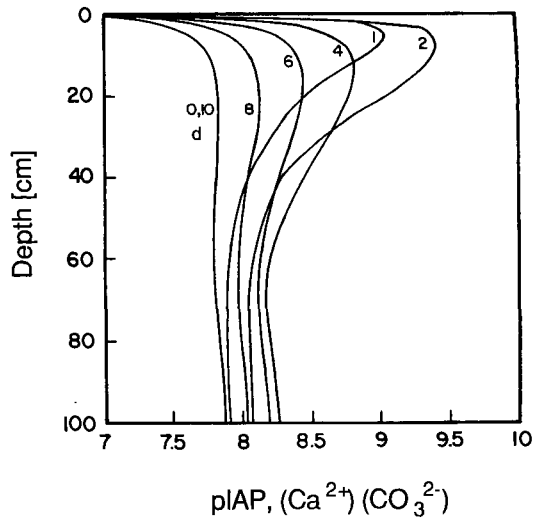

Fig. 13. Calcium carbonate pIAP (ion activity product) values with depth for a 10-d irrigation cycle after 1-yr simulation of irrigation and plant water uptake using Colorado River water and kinetic model coupled to CO_2 production–transport submodel. The value pIAP = 8.48 represents calcite equilibrium condition.

model change less than the corresponding Ca changes shown in Fig. 11, because Ca concentrations were greater than alkalinity concentrations in the irrigation water. This ion imbalance causes a buffering effect on the minor ion and allows larger fluctuation of the dominant ion.

The differences in Ca and alkalinity concentration between the equilibrium and kinetic models are consistent with the pIAP changes presented in Fig. 13 for the same 10-d cycle. Changes in pH with depth and time are also quite variable, as shown in Fig. 14 for the kinetic model. This range in pH has important implications for plant nutrition as well as chemical transport.

CONCLUSION

The model presented attempts a realistic representation of the dynamic processes operating on the soil solution composition of arid land and nonacidic soils. It contains several unique features such as the prediction of CO_2 pressure, pH, inclusion of the constant capacitance model for pH-dependent B adsorption, consideration of the effect of solution composition on hydraulic properties, and inclusion of kinetic rather than equilibrium expressions for reactions where equilibrium cannot be assumed. Consideration of both calcite kinetics and CO_2 production and transport was demonstrated to have important effects on solution composition as well as on the quantity and location of inorganic C precipitation–dissolution in the soil profile. The dynamic nature of the soil solution composition also results in differences in the changes experienced by different ions, and differences in changes depending on depth. Most soil solution sampling strategies are not designed to capture this variation.

Some aspects of the model can be considered concep-

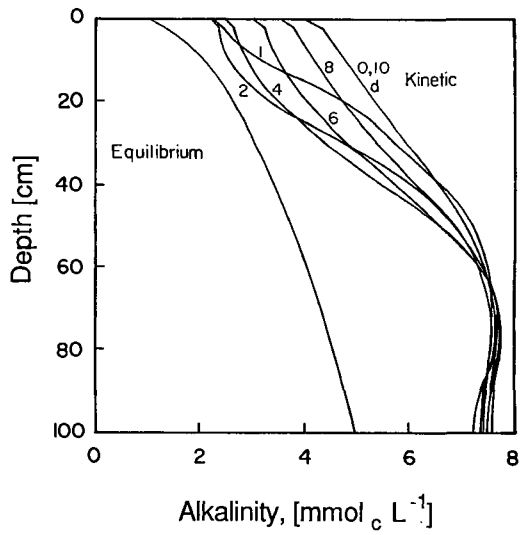

Fig. 12. Alkalinity concentration profiles with depth for a 10-d irrigation cycle after 1-yr simulation of irrigation and plant water uptake using Colorado River water (a) calcite equilibrium condition and (b) kinetic model coupled to CO_2 production–transport submodel.

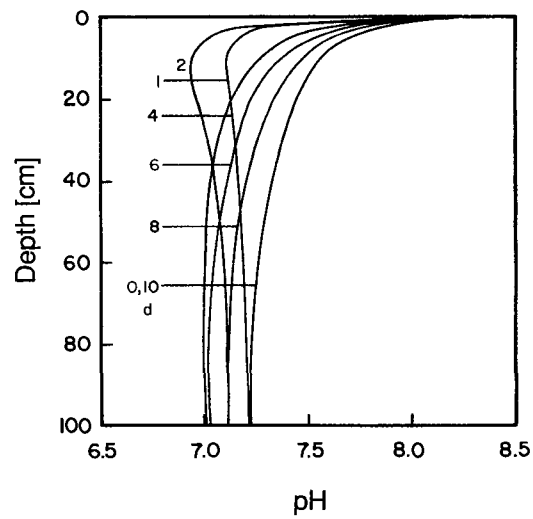

Fig. 14. Soil water pH values with depth for a 10-d irrigation cycle after 1-yr simulation of irrigation and plant water uptake using Colorado River water and kinetic model coupled to CO_2 production–transport submodel.

tual in that individual parts have been determined experimentally but they have not yet been evaluated within an integrated system. In addition to needed evaluation of the model with field studies, it is our objective to incorporate into the model additional solid-phase reactions including evaporite minerals.

APPENDIX

The chemical system includes nine major aqueous components [Ca^{2+}, Mg^{2+}, Na^+, K^+, CO_3^{2-}, SO_4^{2-}, Cl^-, $B(OH)_3$, and H_4SiO_4], 13 complexed species [$CaCO_3^0$, $CaHCO_3^-$, $CaSO_4^0$, $MgCO_3^0$, $MgHCO_3^-$, $MgSO_4^0$, $NaCO_3^-$, $NaHCO_3^0$, $NaSO_4^-$, KSO_4^-, $B(OH)_4^-$, $H_3SiO_4^-$, and $H_2SiO_4^{2-}$], six precipitated species (calcite, gypsum, dolomite, nesquehonite, hydromagnesite, and sepiolite), five sorbed species ($\overline{Ca}$, $\overline{Mg}$, $\overline{Na}$, $\overline{K}$, and SH_2BO_3), and five additional species (pCO_2, $H_2CO_3^*$, HCO_3^-, H^+, and OH^-). Altogether we consider 38 species, and therefore we define 38 independent equations to solve this system.

Carbon Dioxide–Water System

The dissociation reaction of water is written as

$$H_2O \rightleftharpoons H^+ + OH^- \qquad K_W = \frac{(H^+)(OH^-)}{(H_2O)} \qquad [A1]$$

where K_W is the dissociation constant for water and brackets ( ) denote ion activity.

The solubility of $CO_2(g)$ in water is given by

$$H_2CO_3^* \rightleftharpoons CO_{2(g)} + H_2O$$

$$K_{CO_2} = \frac{(H_2CO_3^*)}{(CO_{2(g)})(H_2O)} = \frac{(H_2CO_3^*)}{p_{CO_2}(H_2O)} \qquad [A2]$$

where the activity of $CO_2(g)$ is expressed in terms of the partial pressure pCO_2, K_{CO_2} is Henry's law constant, and $H_2CO_3^*$ represents both CO_2 aqueous and H_2CO_3. Protolysis reactions of dissolved CO_2 are written as

$$H_2CO_3^* \rightleftharpoons H^+ + HCO_3^- \qquad K_{a_1} = \frac{(HCO_3^-)(H^+)}{(H_2CO_3^*)} \qquad [A3]$$

$$HCO_3^- \rightleftharpoons H^+ + CO_3^{2-} \qquad K_{a_2} = \frac{(CO_3^{2-})(H^+)}{(HCO_3^-)} \qquad [A4]$$

where K_{a_1} and K_{a_2} are the first and the second dissociation constant of H_2CO_3.

REFERENCES

Amrhein, C., and D.L. Suarez. 1988. The use of a surface complexation model to describe the kinetics of ligand-promoted dissolution of anorthite. Geochim. Cosmochim. Acta 52:2785–2793.

Baes, A.U., and P.R. Bloom. 1988. Exchange of divalent cations in soil organic matter. Soil Sci. 14:6–14.

Ball, J.W., D.K. Nordstrom, and D.W. Zachmann. 1987. WATEQ4F — A personal computer FORTRAN translation of the geochemical model WATEQ2 with revised data base. U.S. Geol. Surv. Open File Rep. 87 50. U.S. Geol. Surv., Menlo Park, CA.

Bell, R.P., and J.H.B. George. 1953. Dissociation of thallus and Ca sulfate salts at different temperatures. Trans. Faraday Soc. 49: 619–627.

Bresler, E. 1973. Simultaneous transport of solute and water under transient unsaturated flow conditions. Water Resour. Res. 9:975–986.

Busenberg, E., and L.N. Plummer. 1982. The kinetics of dissolution of dolomite in CO_2–H_2O systems at 1.5 to 65°C and 0 to 1 atm P_{CO_2}. Am. J. Sci. 282:45–78.

Buyanovsky, G.A., and G.H. Wagner. 1983. Annual cycles of carbon dioxide in soil air. Soil Sci. Soc. Am. J. 47:1139–1245.

Chou, L., and R. Wollast. 1985. Steady-state kinetics and dissolution mechanisms of albite. Am. J. Sci. 285:963–993.

Clesceri, L.S., A.E. Greenberg, and R.R. Trussell (ed.). 1989. Silica. p. 4-181 to 4-191. *In* Standard methods for the examination of water and wastewater. 17th ed. Am. Public Health Assoc., Washington, DC.

Dudley, L.M., R.J. Wagenet, and J.J. Jurinak. 1981. Description of soil chemistry during transient solute transport. Water Resour. Res. 17:1498–1504.

Felmy, A.R., and J.H. Weare. 1986. The prediction of borate mineral equilibria in natural waters: Application to Searles Lake, California. Geochim. Cosmochim. Acta 50:2771–2783.

Förster, R., and H. Gerke. 1988. Integration von Modellen des Wasser- und Stofftransports sowie physikochemischer Wechselwirkungen zur Analyse von Agrar-Ökosystemen. Verh. Ges. Oekol. 18: 515–522.

Frenkel, H., J.O. Goertzen, and J.D. Rhoades. 1978. Effects of clay type and content, exchangeable sodium percentage and electrolyte concentration on clay dispersion and soil hydraulic conductivity. Soil Sci. Soc. Am. J. 42:32–39.

Furrer, G., and W. Stumm. 1986. The coordination chemistry of weathering: I. Dissolution kinetics of δ Al_2O_3 and BeO. Geochim. Cosmochim. Acta 50:1847–1860.

Goldberg, S. 1993. Chemistry and mineralogy of boron in soils p. 3–44. *In* U.C. Gupta (ed.) Boron and its role in crop production. CRC Press, Ann Arbor, MI.

Goldberg, S., and R.A. Glaubig. 1985. Boron adsorption on aluminum and iron oxide minerals. Soil Sci. Soc. Am. J. 49:1374–1379.

Hillel, D., and C.H.M. van Bavel. 1976. Simulation of profile water storage as related to soil hydrologic properties. Soil Sci. Soc. Am. J. 40:807–815.

Inskeep, W.P., and P.R. Bloom. 1985. An evaluation of rate equations for calcite precipitation kinetics at pCO_2 less than 0.01 atm and pH greater than 8. Geochim. Cosmochim. Acta 49:2165–2180.

Inskeep, W.P., and P.R. Bloom. 1986. Kinetics of calcite precipitation in the presence of water-soluble organic ligands. Soil Sci. Soc. Am. J. 50:1167–1172.

Jacobson, R.L. 1973. Controls on the quality of some carbonate groundwaters: Dissociation constants of calcite and $CaHCO_3^+$ from 0 to 50°C. Ph.D. diss. Pennsylvania State Univ., University Park (Diss. Abstr. 74-04250).

Jennings, A.A., D.J. Kirkner, and T.L. Theis. 1982. Multicomponent equilibrium chemistry in groundwater quality models. Water Resour. Res. 18:1089–1096.

Jury, W.A., H. Frenkel, and L.H. Stolzy. 1978. Transient changes in the soil water system from irrigation with saline water: I. Theory. Soil Sci. Soc. Am. J. 42:579–584.

Lebron, I., and D.L. Suarez. 1996. Calcite nucleation and precipitation kinetics as affected by dissolved organic matter at 25°C and pH > 7.5. Geochem. Cosmochim Acta 60:2765–2776.

McNeal, B.L. 1968. Prediction of the effect of mixed-salt solutions on soil hydraulic conductivity. Soil Sci. Soc. Am. Proc. 32:190–193.

Miller, C.W., and L.V. Benson. 1983. Simulation of solute transport in a chemically reactive heterogeneous system: Model development and application. Water Resour. Res. 19:381–391.

Mualem, Y. 1976. A new model for predicting the hydraulic conductivity of unsaturated porous media. Water Resour. Res. 12:513–522.

Narasimhan, T.N., A.F. White, and T. Tokunaga. 1986. Groundwater contamination from an inactive uranium mill tailings pile. 2: Application of a dynamic mixing model. Water Resour. Res. 22: 1820–1834.

Pratt, P.F. 1957. The effect of fertilizers and organic materials on the cation-exchange capacity of an irrigated soil. Soil Sci. 83:85–89.

Pitzer, K.S. 1979. Theory: Ion interaction approach. p. 157–208. *In* R.M. Pytkowicz (ed.) Activity coefficients in electrolyte solutions. Vol. 1. CRC Press, Boca Raton, FL.

Plummer, L.N., and E. Busenberg. 1982. The solubilities of calcite, aragonite and vaterite in CO_2–H_2O solutions between 0 and 90°C, and an evaluation of the aqueous model for the system $CaCO_3$–CO_2–H_2O. Geochim. Cosmochim. Acta 46:1011–1040.

Plummer, L.N., T.M. Wigley, and D.L. Parkhurst. 1978. The kinetics of calcite dissolution in CO_2 systems at 5° to 60°C and 0.0 to 1.0 atm CO_2. Am. J. Sci. 278:179–216.

Reardon, E.J. 1974. Thermodynamic properties of some sulfate, car-

bonate and bicarbonate ion pairs. Ph.D. diss. Pennsylvania State Univ., University Park (Diss. Abstr. 75-09830).

Reardon, E.J., and D. Langmuir. 1974. Thermodynamic properties of the ion pairs $MgCO_3^0$ and $CaCO_3^0$ from 10 to 50°C. Am. J. Sci. 274:599–612.

Reardon, E.J., and D. Langmuir. 1976. Activity coefficients of $MgCO_3^0$ and $CaSO_4^0$ ion pairs as a function of ionic strength. Geochim. Cosmochim. Acta 40:549–554.

Robbins, C.W., R.J. Wagenet, and J.J. Jurinak. 1980a. A combined salt transport–chemical equilibrium model for calcareous and gypsiferous soils. Soil Sci. Soc. Am. J. 44:1191–1194.

Robbins, C.W., R.J. Wagenet, and J.J. Jurinak. 1980b. Calculating cation exchange in a salt transport model. Soil Sci. Soc. Am. J. 44:1195–1200.

Robinson, R.A., and R.H. Stokes. 1965. Electrolyte solutions. Butterworths, London.

Russo, D. 1986. Simulation of leaching of a gypsiferous–sodic desert soil. Water Resour. Res. 22:1341–1349.

Schulz, H.D., and E.J. Reardon. 1983. A combined mixing cell/analytical model to describe two-dimensional reactive solute transport for unidirectional groundwater flow. Water Resour. Res. 19:493–502.

Šimůnek, J., and D.L. Suarez. 1993. Modeling of carbon dioxide transport and production in soil: 1. Model development. Water Resour. Res. 29:487–497.

Šimůnek, J., and D.L. Suarez. 1994. Two-dimensional transport model for variably saturated porous media with major ion chemistry. Water Resour. Res. 30:1115–1133.

Stumm, W., and J.J. Morgan. 1981. Aquatic chemistry: An introduction emphasizing chemical equilibria in natural waters. John Wiley & Sons, New York.

Suarez, D.L. 1977a. Ion activity products of calcium carbonate in waters below the root zone. Soil Sci. Soc. Am. J. 41:310–315.

Suarez, D.L. 1977b. Magnesium, carbonate, and silica interactions in soils. U.S. Salinity Lab. Annual Rep. USDA-ARS, U.S. Salinity Lab., Riverside, CA.

Suarez, D.L. 1983. Calcite supersaturation and precipitation kinetics in the lower Colorado River, All-American Canal and Highline Canal. Water Resour. Res. 19:653–661.

Suarez, D.L. 1985. Prediction of major ion concentrations in arid land soils using equilibrium and kinetic theories. *In* D. DeCoursey (ed.) Proc. Nat. Resour. Modeling Symp., Pingree Park, CO. 1983. USDA-ARS-30. U.S. Gov. Print. Office, Washington, DC.

Suarez, D.L., A.M. Aboushal, and J.D. Wood. 1994. Predicting Ca–Na exchange selectivities of smetitic soils. p. 258. *In* Agronomy abstracts. ASA, Madison, WI.

Suarez, D.L., J.D. Rhoades, R. Lavado, and C.M. Grieve. 1984. Effect of pH on saturated hydraulic conductivity and soil dispersion. Soil Sci. Soc. Am. J. 48:50–55.

Suarez, D.L., and J. Šimůnek. 1993. Modeling of carbon dioxide transport and production in soil: 2. Parameter selection, sensitivity analysis and comparison of model predictions to field data. Water Resour. Res. 29:499–513.

Suarez, D.L., and J.D. Wood. 1993. Predicting Ca–Mg exchange selectivities of smetitic soils. p. 236. *In* Agronomy abstracts. ASA, Madison, WI.

Suarez, D.L., and J.D. Wood. 1996. Short- and long-term weathering rates of a feldspar fraction isolated from an arid zone soil. Chem. Geol. 132:143–150.

Suarez, D.L., J.D. Wood, and I. Ibrahim. 1992. Reevaluation of calcite supersaturation in soils. Soil Sci. Soc. Am. J. 56:1776–1784.

Suarez, D.L., and M. Zahow. 1989. Calcium–magnesium exchange selectivity of Wyoming montmorillonite in chloride, sulfate, and perchlorate solutions. Soil Sci. Soc. Am. J. 53:52–57.

Sverdrup, H.U., and P. Warfvinge. 1988. Weathering of primary silicate minerals in the natural soil environment in relation to a chemical weathering model. Water Air Soil Pollut. 38:397–408.

Swoboda-Colberg, N.G., and J.I. Drever. 1993. Mineral dissolution rates in plot-scale field and laboratory experiments. Chem. Geol. 105:51–69.

Truesdell, A.H., and B.F. Jones. 1974. Wateq, a computer program for calculating chemical equilibria of natural waters. J. Res. U.S. Geol. Surv. 2:233–248.

van Genuchten, M.Th. 1980. A closed-form equation for predicting the hydraulic conductivity of unsaturated soils. Soil Sci. Soc. Am. J. 44:892–898.

Wagenet, R.J., and J.L. Hutson. 1987. LEACHM: A finite-difference model for simulating water, salt, and pesticide movement in the plant root zone. Continuum 2. N.Y. State Resour. Inst., Cornell Univ., Ithaca, NY.

Walsh, M.P., S.L. Bryant, R.S. Schechter, and L.W. Lake. 1984. Precipitation and dissolution of solids attending flow through porous media. AIChE J. 30:317–328.

White, N., and L.W. Zelazny. 1986. Charge properties in soil colloids. p. 39–81. *In* D.L. Sparks (ed.) Soil physical chemistry. CRC Press, Boca Raton, FL.

Yeh, G.T., and V.S. Tripathi. 1989. A critical evaluation of recent developments in hydrogeochemical transport models of reactive multichemical components. Water Resour. Res. 25:93–108.

Yeh, G.T., and V.S. Tripathi. 1991. A model for simulating transport of reactive multispecies components: Model development and demonstration. Water Resour. Res. 27:3075–3094.